Evidence of dual energy transfer driven by magnetic reconnection at subion scales

Raffaello Foldes ⬤[*]

CNRS, École Centrale de Lyon, INSA de Lyon, Université Claude Bernard Lyon 1,
Laboratoire de Mécanique des Fluides et d'Acoustique, F-69134 Écully, France

Silvio Sergio Cerri ⬤[†]

Université Côte d'Azur, Observatoire de la Côte d'Azur, CNRS, Laboratoire Lagrange, Bd de l'Observatoire,
CS 34229, 06304 Nice cedex 4, France

Raffaele Marino ⬤[‡]

CNRS, École Centrale de Lyon, INSA de Lyon, Université Claude Bernard Lyon 1, Laboratoire de Mécanique
des Fluides et d'Acoustique, F-69134 Écully, France

Enrico Camporeale[§]

School of Physical and Chemical Sciences, Queen Mary University of London, London E1 4NS, United Kingdom
and Space Weather Technology, Research and Education Center (SWx-TREC), University of Colorado, Boulder, Colorado 80309, USA

The properties of energy transfer in the kinetic range of plasma turbulence have fundamental implications on the turbulent heating of space and astrophysical plasmas. It was suggested that magnetic reconnection may be responsible for driving the subion scale cascade, and that this process would be characterized by a direct energy transfer toward even smaller scales (until dissipation), and a simultaneous inverse transfer of energy toward larger scales, until the ion break. Here we employ the space-filter technique on high-resolution 2D3V hybrid-Vlasov simulations of continuously driven turbulence providing quantitative evidence that magnetic reconnection is indeed able to trigger a dual energy transfer originating at subion scales.

I. INTRODUCTION

Investigations of kinetic-scale plasma turbulence have seen a surge of interest in the past decade, driven by increasingly accurate *in situ* measurements in such range [1–6]. In this context, a transition between magnetohydrodynamic (MHD) and kinetic regimes occurs when the forward-cascading turbulent energy reaches ion scales [7]. Extensive numerical campaigns have recently been performed in order to better understand the properties of turbulence and plasma heating across and below the so-called ion break, targeting the interplanetary medium [8–22]. Based on these simulation results, it has been speculated that magnetic reconnection might be at the origin of the observed ion-break formation driving the subsequent subion scale cascade [23,24]. Such conjecture has been supported at least partially by solar-wind observations [25]. Since then, tearing-mediated turbulence has been the subject of thorough numerical investigations [26–31]. Yet, the role of reconnection in the energy transfer across and below the ion scales remains rather elusive. As we show in this article, an effective approach to tackle potentially relevant transfer mechanisms is provided by the so-called space-filter technique, originally developed in the context of hydrodynamics for "large-eddy simulations" [32,33], and later on adopted as an investigative tool in plasma turbulence [34–44]. A qualitative picture of the kinetic-range energy transfer in a tearing-mediated scenario was suggested in Franci *et al.* [24] (see their Fig. 4). In that work, the interaction between large-scale vortices feeding the formation of strong current sheets at their boundaries, quickly destroyed by the plasmoid instability, was interpreted as a nonlocal transfer of energy from the large scales (of the vortices) directly to subion scales (comparable to the thickness of the current sheets). Moreover, the continuous formation of small-scale magnetic islands (plasmoids) and their subsequent merging to form bigger structures was interpreted as an inverse transfer toward larger scales. Thus, a dual transfer of energy should develop at subion scales: a direct transfer of reconnection-induced fluctuations toward smaller scales until dissipation, and a simultaneous inverse transfer toward the ion break due to the plasmoid growth by island coalescence. This picture has been purely qualitative until now, the presence of bidirectional energy transfers being previously assessed in MHD plasmas [45] as well as in rotating-stratified geophysical fluids [46–49].

Here, 2D3V hybrid-kinetic simulations of forced turbulence are analyzed by means of a space-filter technique, which allows to investigate the (local and nonlocal) energy transfer in kinetic plasmas through scales as a function of spatial

---

[*]Contact author: raffaello.foldes@ec-lyon.fr
[†]Contact author: silvio.cerri@oca.eu
[‡]Contact author: raffaele.marino@ec-lyon.fr
[§]Contact author: enrico.camporeale@qmul.ac.uk

location and time. Though unable to capture full small-scale dynamics of three-dimensional plasmas, 2.5D hybrid-kinetic simulations have proven to be an adequate starting point to investigate several aspects of space plasma turbulence, along with Hall-MHD simulations [50]. They are indeed able to reproduce features like the intermittent character of turbulent energy transfer and dissipation in the solar wind [51–53] and several kinetic-scale spectral features [e.g., 44,54]. We show how the occurrence of magnetic reconnection (i) enables a consistent energy transfer below ion scales, and (ii) drives a dual (inverse and direct) transfer within the subion range.

II. METHOD

We analyze the 2D3V hybrid-Vlasov-Maxwell (HVM) simulation of continuously driven turbulence in a $\beta_i = \beta_e = 1$ plasma presented in Cerri and Califano [23]. The HVM model evolves fully kinetic ions, solving the Vlasov equation for their distribution function $f_i(\boldsymbol{x}, \boldsymbol{v}, t)$, and fluid electrons through a generalized Ohm's law in the quasineutral approximation $n_i = n_e \doteq n$ (displacement current in the Ampère's law is neglected). The simulation size is 1024^2 grid points in real space, spanning a wavenumber range $0.1 \leqslant kd_i \leqslant 51.2$, where $k = k_\perp = (k_x^2 + k_y^2)^{1/2}$ and d_i is the ion inertial length. An external forcing in the Vlasov equation continuously injects ion-momentum fluctuations at scales $0.1 \leqslant k_{ext}d_i \leqslant 0.2$; the magnetic field is initialized (at $t = 0$) with small-amplitude perturbations $\delta\boldsymbol{B}$ at wavenumbers $0.1 \leqslant k_{\delta B}d_i \leqslant 0.3$, reaching $\delta B_{rms}/B_0 \sim 0.1$ in the quasisteady state. Results from this HVM simulation were used to conjecture the existence of a sub-ion-scale tearing-mediated range [23]; they were later accompanied by a hybrid-PIC simulation to confirm such conjecture [24]. Although the fluctuations' properties have been thoroughly analyzed [55], a detailed analysis of the turbulent energy transfer based on this high-resolution numerical simulation had to await the development of a proper space-filter formalism and diagnostics for hybrid-kinetic models [40].

In the following, a filtered vector field $\widetilde{V}(\boldsymbol{x}, t)$ denotes the convolution of $V(\boldsymbol{x}, t)$ with a filter φ, i.e., $\widetilde{V}(\boldsymbol{x}, t) \doteq \int_\Omega \varphi(x - \xi)V(\boldsymbol{x}, t)d\xi$ over the domain Ω. Here, we adopt the low-pass Butterworth filter, which in Fourier space reads $\varphi_k = 1/[1 + (k/k_*)^8]$ with $k_* (\sim \ell_*^{-1})$ being the characteristic filtering wavenumber (scale). The Favre filter of V is $\widehat{V} \doteq \widetilde{\varrho V}/\widetilde{\varrho}$, where ϱ is the mass density. Filtered equations for the energy channels in general quasineutral hybrid-kinetic models are presented in [40]. When dissipation and external injection can be neglected in the HVM model with massless, isothermal electrons, these equations read

$$\frac{\partial \langle \widehat{\mathcal{E}}_{u_i} \rangle}{\partial t} = \langle \widehat{\Phi}_{u_i, B} \rangle + \langle \widehat{\Phi}_{u_i, \Pi_i} \rangle - \langle \mathcal{S}_{u_i} \rangle, \qquad (1)$$

$$\frac{\partial \langle \widehat{\mathcal{E}}_{\Pi_i} \rangle}{\partial t} = -\langle \widehat{\Phi}_{u_i, \Pi_i} \rangle - \langle \mathcal{S}_{\Pi_i} \rangle, \qquad (2)$$

$$\frac{\partial \langle \widehat{\mathcal{E}}_B \rangle}{\partial t} = \langle \widehat{\mathcal{I}}_e \rangle - \langle \widehat{\Phi}_{u_i, B} \rangle - \langle \mathcal{S}_B \rangle, \qquad (3)$$

where $\langle \dots \rangle$ denotes a spatial average, $\widehat{\mathcal{E}}_{u_i} = \frac{1}{2}\widetilde{\varrho}|\widehat{\boldsymbol{u}}_i|^2$, $\widehat{\mathcal{E}}_{\Pi_i} = \frac{1}{2}\mathrm{tr}[\widehat{\boldsymbol{\Pi}}_i]$, and $\widehat{\mathcal{E}}_B = |\widehat{\boldsymbol{B}}|^2/8\pi$ are the ion-kinetic, ion-thermal,

and magnetic energy densities at scales $\ell \geqslant \ell_*$, respectively ($\boldsymbol{\Pi}_i$ is the ion-pressure tensor and $\boldsymbol{u}_i$ is the ion-bulk flow, both obtained as $\boldsymbol{v}$-space moments of f_i). The injectionlike term $\widehat{\mathcal{I}}_e \doteq \widetilde{P}_e(\nabla \cdot \widehat{\boldsymbol{u}}_e)$ involving scales $\ell \geqslant \ell_*$ is due to the isothermal-electron condition $P_e = nT_{0,e}$. The terms $\widehat{\Phi}_{u_i, B} \doteq \widehat{\boldsymbol{j}}_i \cdot \widehat{\boldsymbol{E}}$ (where $\widehat{\boldsymbol{j}}_i = e n \widehat{\boldsymbol{u}}_i$) and $\widehat{\Phi}_{u_i, \Pi_i} \doteq \widehat{\boldsymbol{\Pi}}_i : \nabla \widehat{\boldsymbol{u}}_i$ represent energy exchange (i.e., conversion) between different channels (occurring at scales $\ell \geqslant \ell_*$). Finally, the source/sink terms representing the (local and nonlocal) energy transfer between large ($k < k_*$) and small ($k > k_*$) scales through the filtering scale $k_* \sim \ell_*^{-1}$ are

$$\mathcal{S}_{u_i} \doteq \widehat{\boldsymbol{j}}_i \cdot \boldsymbol{\epsilon}_{MHD}^* - \boldsymbol{\mathcal{T}}_{uu}^{(i)} : \nabla \widehat{\boldsymbol{u}}_i, \qquad (4)$$

$$\mathcal{S}_{\Pi_i} \doteq \mathcal{T}_{\Pi\nabla u}^{(i)}, \qquad (5)$$

$$\mathcal{S}_B \doteq \widehat{\boldsymbol{j}}_e \cdot (\boldsymbol{\epsilon}_{MHD}^* + \boldsymbol{\epsilon}_{Hall}^*) + \boldsymbol{j}^* \cdot \widehat{\boldsymbol{E}}, \qquad (6)$$

where $\widehat{\boldsymbol{j}}_e = -e n \widehat{\boldsymbol{u}}_e = \widetilde{\boldsymbol{J}} - e n \widehat{\boldsymbol{u}}_i$ (with $\widetilde{\boldsymbol{J}} = \frac{c}{4\pi}\nabla \times \widetilde{\boldsymbol{B}}$), and we have introduced the "turbulent" electric fields and current density at scales $\ell < \ell_*$, $\boldsymbol{\epsilon}_{MHD}^* = -\boldsymbol{\mathcal{T}}_{u \times B}^{(i)}$, $\boldsymbol{\epsilon}_{Hall}^* = -\boldsymbol{\mathcal{T}}_{J \times B}$, and $\boldsymbol{j}^* = \boldsymbol{\mathcal{T}}_{nu}^{(i)} - \boldsymbol{\mathcal{T}}_{nu}^{(e)} = \widehat{\boldsymbol{J}} - \widetilde{\boldsymbol{J}}$. The sign convention is such that $\mathcal{S} > 0$ denotes direct energy transfer from large to small scales, while $\mathcal{S} < 0$ means inverse transfer from small to large scales. The "subgrid" terms $\mathcal{T}$ associated to nonlinearities are given by $\boldsymbol{\mathcal{T}}_{uu}^{(i)} \doteq \widetilde{\varrho}(\widehat{\boldsymbol{u}_i\boldsymbol{u}_i} - \widehat{\boldsymbol{u}}_i\widehat{\boldsymbol{u}}_i)$, $\boldsymbol{\mathcal{T}}_{u \times B}^{(i)} = \frac{1}{c}(\widehat{\boldsymbol{u}_i \times \boldsymbol{B}} - \widehat{\boldsymbol{u}}_i \times \widehat{\boldsymbol{B}})$, $\boldsymbol{\mathcal{T}}_{\Pi\nabla u}^{(i)} \doteq \widehat{\Pi_{i,jk}\partial_k u_{i,j}} - \widehat{\Pi}_{i,jk}\partial_k\widehat{u}_{i,j}$, $\boldsymbol{\mathcal{T}}_{J \times B} \doteq \frac{m_i}{ec}\frac{1}{\widetilde{\varrho}}(\widehat{\boldsymbol{J} \times \boldsymbol{B}} - \widehat{\boldsymbol{J}} \times \widetilde{\boldsymbol{B}})$, and $\boldsymbol{\mathcal{T}}_{nu}^{(\alpha)} \doteq \widehat{n\boldsymbol{u}_\alpha} - \widetilde{n}\widehat{\boldsymbol{u}}_\alpha$. The corresponding equation for the (filtered) total energy $\widehat{\mathcal{E}} = \widehat{\mathcal{E}}_{u_i} + \widehat{\mathcal{E}}_{\Pi_i} + \widehat{\mathcal{E}}_B$ is $\partial_t\langle \widehat{\mathcal{E}} \rangle = \langle \widehat{\mathcal{I}}_e \rangle - \langle \mathcal{S}_{tot} \rangle$, where $\mathcal{S}_{tot} = \mathcal{S}_{u_i} + \mathcal{S}_{\Pi_i} + \mathcal{S}_B$. In the following, we focus our analysis on the terms $\mathcal{S}$, representing the actual transfer through scales.

III. RESULTS

The simulation exhibits two noteworthy times (in inverse ion-cyclotron frequency units $\Omega_{c,i}^{-1}$): the time of first reconnection events $t_{rec} \approx 135$, and the time marking the transition to quasisteady turbulence $t_{qst} \approx 200$ (Fig. 1 of [24]). Here, we analyze features of the flux terms computed throughout the simulation domain as the plasma dynamics evolve. In order to locate the most prominent reconnection sites, we focus on subregions characterized by the highest (on average) values of the current density and the formation of the largest number of plasmoids, indicated as box 1 and box 2 in Fig. 1. The left panel shows contours of the out-of-plane current density J_z/σ_{J_z} at $t \simeq 206$, alongside contours of the total-energy transfer $\mathcal{S}_{tot}/\sigma_{\mathcal{S}_{tot}}$ (both normalized by their standard deviations) through two representative wavenumbers, $kd_i = 2.5$ and $kd_i = 5.5$. To highlight spatial correlations between current structures and total-energy transfer, a movie of Fig. 1 can be found in the Supplemental Material [56]. These renderings emphasize qualitatively the key result of our analysis: as k increases, the energy transfer becomes significantly less volume filling and more localized within the most intense currents; concurrently, as the time goes by, progressively larger magnetic islands arise from the edge of the current structures [38,39]. These dynamics can be understood as the simultaneous generation of small scales due to the disruption of the (large-scale) current structures by magnetic reconnection,
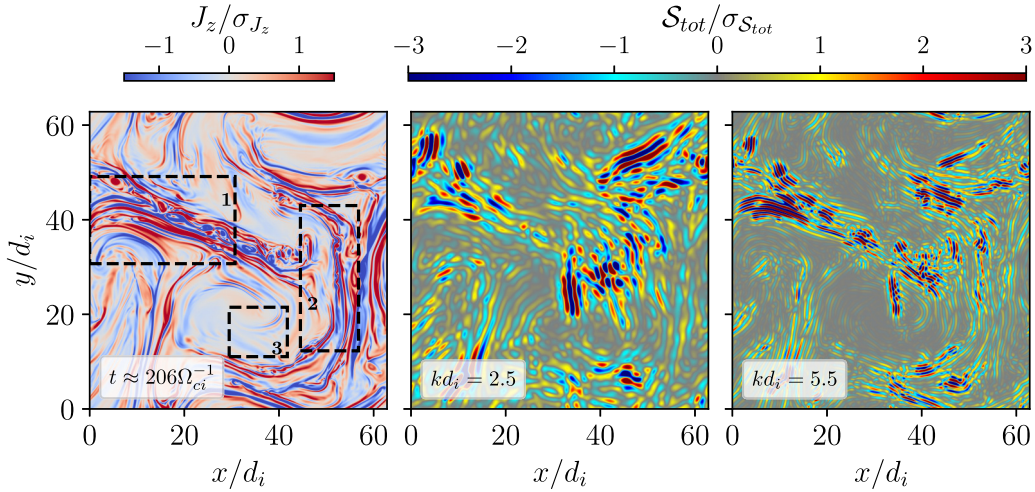
FIG. 1. (Left) Out-of-plane current density $J'_z = J_z/\sigma_J$ at the time $t \approx 206\Omega_{c,i}^{-1}$, when the system reaches a quasisteady state. (Middle) Total energy transfer $\mathcal{S}'_{tot} = \mathcal{S}_{tot}/\sigma_S$ computed at the scales $kd_i = 2.5$ (center) and $kd_i = 5.5$ (right). The dashed boxes 1 and 2 highlight regions with intense reconnection, box 3 is a reference region in which reconnection is absent or very weak.

and the nonlinear growth of mesoscale magnetic islands—corresponding to an upscale energy transfer—that suggests the existence of a bidirectional energy cascade at subion scales. In order to quantitavely assess the local-in-space properties of energy transfer as a function of the scale and in time, as well as to characterize the role of magnetic reconnection, we analyze averages of the flux terms computed on box 1 and 2, and on a subregion pervaded by weaker currents showing no signs of reconnection during the simulation (box 3 in Fig. 1 and in [56]). Such analysis is reported in Fig. 2, where scalograms of the total-energy transfer rate $\langle \mathcal{S}_{tot} \rangle$, averaged over each box, are plotted as a function of kd_i versus simulation time. Red colors in $\langle \mathcal{S}_{tot} \rangle$ correspond to a direct energy transfer from large to small scales, whereas upscale (inverse) transfer is indicated by blue tones. The coexistence of forward and inverse transfers—with a sign inversion occurring in the range $3 \lesssim kd_i \lesssim 4$—demonstrates the existence of a dual cascade, active at subion scales in box 1 and box 2, which is likely triggered by magnetic reconnection. The latter is inferred through the time evolution of the root-mean-square current density J_{rms} within each box (black lines overlaid on the scalograms). In particular, the dual cascade seems to set at those times when J_{rms} roughly saturates, $t \simeq 160$ and $t \simeq 180$ in box 1 and box 2, respectively. Box 3 is instead characterized by a nearly flat current signal with relatively low intensity, indicative of no clear reconnection activity.

In this subregion, the sign of $\langle \mathcal{S}_{tot} \rangle$ switches rapidly between positive and negative values as the time goes by, with most of the total energy transfer being concentrated at scales $kd_i \lesssim 2$ though with strong oscillations. For $t \gtrsim 210$, the inverse energy transfer in both box 1 and box 2 becomes more sparse and less intense, which might be due to the presence of constant ion energization/heating processes as the system settles to a fully developed turbulent state. As reported by Lu *et al.* [57], a reduction of the reconnection rate may indeed be the consequence of the enhanced ion pressure induced by turbulent forcing. Another possibility is that in our setup the typical timescale over which the system will reform the

current sheets is related to the relatively long eddy turnover time set by the forcing ($\tau_{nl} \sim 120\,\Omega_{c,i}^{-1}$); thus, intense bursts of reconnection events can occur only on those timescales. These evidences, including the absence in box 3 of energy transfer at scales $kd_i > 2$ and no extended segments characterized by definite sign, further support the interpretation that the subion dual cascade is triggered by reconnection events when their intensity attains a certain threshold. Scalograms of the channel-specific transfer rates, $\langle \mathcal{S}_B \rangle$, $\langle \mathcal{S}_{u_i} \rangle$, and $\langle \mathcal{S}_{\Pi_i} \rangle$, averaged over each box, as well as the scalograms of $\langle \mathcal{S}_{tot} \rangle$ and channel-specific transfer averaged over the entire simulation domain, can be found in the Supplemental Material [58]. It is worth mentioning that, when averaged over the entire box, in our simulation the dual cascade becomes more intermittent in time, typically emerging only after local peaks in the rms current density; how this feature depends on the system size L, on the eddy turnover time set by the forcing, and on the outer-scale fluctuations' amplitude is out of the scope of the present work and will require further investigations.

The filtered energy source/sink and exchange terms have been computed point-wise throughout the simulation, then averaged over the boxes indicated in Fig. 1 within a time interval of roughly $165\Omega_{c,i}^{-1}$ from $t \approx 200\Omega_{c,i}^{-1}$, during which the system is reaching a quasisteady state. Figure 3 shows the estimates for box 1, panels (a)–(d), and box 2, panels (e)–(h), in which plasma dynamics are likely driven by magnetic reconnection. The main result of this analysis is reported in the first column, displaying the the total energy transfer $\langle \mathcal{S}_{tot} \rangle$. Two important features emerge from panels (a) and (e): the existence of a simultaneous direct ($\langle \mathcal{S}_{tot} \rangle > 0$) and inverse ($\langle \mathcal{S}_{tot} \rangle < 0$) transfer occurring at subion scales, in the range $1 \lesssim kd_i \lesssim 20$; a forward energy transfer developing at scales $kd_i \lesssim 1$, as expected in the magnetohydrodynamic regime (blue shaded), downstream of the forcing range (gray shaded, together with the dissipative range). From panels (b) and (f) one infers that the bidirectional flux of total energy $\langle \mathcal{S}_{tot} \rangle$ below the ion scale is indeed dominated by the magnetic energy $\langle \mathcal{S}_B \rangle$. The latter is in turn mostly sustained by $\tilde{\boldsymbol{j}}_e \cdot \boldsymbol{\epsilon}^*_{Hall}$, thus
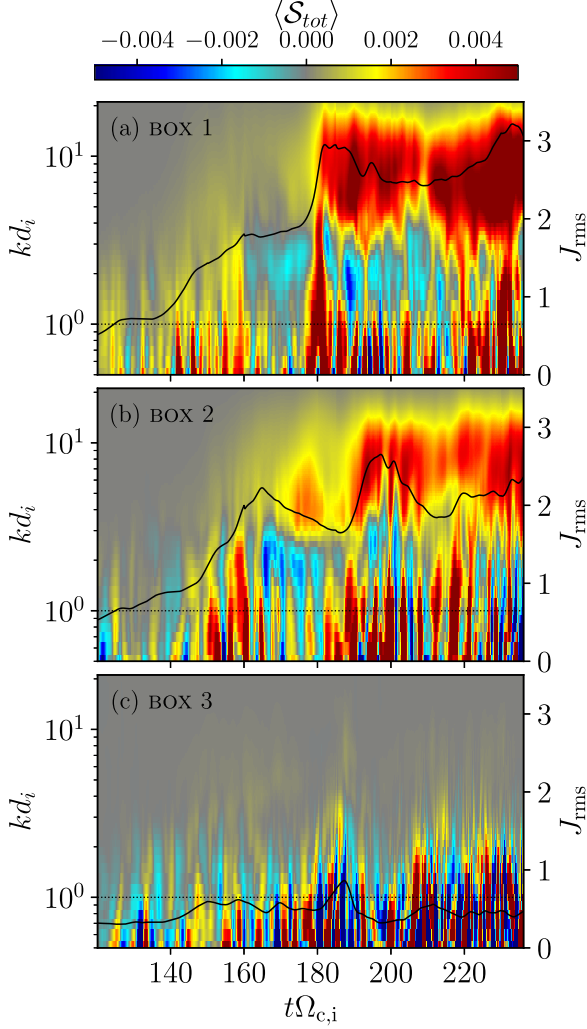
FIG. 2. Temporal evolution of the total energy transfer averaged $\langle \mathcal{S}_{\text{tot}} \rangle$ over the three boxes highlighted in Fig. 1, in the range $0.5 \lesssim kd_i \lesssim 20$. Plasma regions in boxes 1 and 2 develop the most intense reconnection events, while no intense current sheets can be detected in box 3. Black curves are the root-mean-square current density averaged in the corresponding subdomains.

by the coupling of the electron currents with the turbulent Hall electric field. The term $\widehat{\boldsymbol{j}}_e \cdot \boldsymbol{\epsilon}_{\text{MHD}}^*$ contributes instead mostly at larger scale, becoming negligible with respect to the Hall term at $kd_i \gtrsim 5$. The term $\boldsymbol{j}^* \cdot \widehat{\boldsymbol{E}}$ oscillates around zero in the subion range, becoming non-negligible and negative only for $kd_i \lesssim 1$, probably due to the breakup of large-scale current structures by reconnection. On the other hand, negative total and magnetic fluxes at subion scales ($1 \lesssim kd_i \lesssim 4$) are likely associated to the growth of magnetic islands by coalescence, as anticipated in the previous section (see the Supplemental Material [58]). Panels (c) and (g) reveal how the ion-kinetic energy transfer ($\langle \mathcal{S}_{u_i} \rangle$) dominates only within the MHD regime, where it can entirely be accounted for by the coupling of "subgrid" Reynolds stress $\mathcal{T}_{uu}^{(i)}$ and the large-scale strain tensors $\widehat{\boldsymbol{\Sigma}} \doteq \nabla \widehat{\boldsymbol{u}}_i$, $\langle \mathcal{S}_{u_i} \rangle \approx \langle \mathcal{T}_{uu}^{(i)} : \nabla \widehat{\boldsymbol{u}}_i \rangle$. The latter is marginal at scales $kd_i > 2$, the transfer of ion-kinetic energy becoming negligible at scales smaller than their gyroradius [as is observed in the ion-flow spectrum, showing a very steep power

law at subion scales; see, e.g., 54,55,59]. Through the whole range of scales resolved, the conversion of magnetic energy $\widehat{\mathcal{E}}_B$ to ion-bulk energy $\widehat{\mathcal{E}}_{u_i}$ is driven by the large-scale ion current density interaction with the large-scale electric field, being $\widehat{\Phi}_{u_i,B} = \widehat{j}_i \cdot \widehat{E}$, though curves (blue dashed) level off at values with opposite sign, positive for box 1 and negative for box 2. A remark stemming from the comparison of panels (b)–(f) and (c)–(g) is that magnetic ($\langle \mathcal{S}_B \rangle$) and kinetic ($\langle \mathcal{S}_{u_i} \rangle$) energy transfer have comparable amplitudes in the MHD regime, unlike what happens at scales $kd_i \gg 1$, where $\langle \mathcal{S}_B \rangle$ dominates. Finally, panels (d) and (h) show that the ion-thermal energy transfer $\langle \mathcal{S}_{\Pi_i} \rangle$ is only a tiny fraction of the total energy flux, peaking around the forcing wavenumber; interestingly, conversions between ion-thermal energy and ion-kinetic energy ($\widehat{\Phi}_{u_i,\Pi_i}$), like $\widehat{\Phi}_{u_i,B}$ [panels (c) and (g)] saturate at $kd_i \gg 1$. Since the terms $\widehat{\Phi}(k)$ represent the cumulative conversion up to k, their saturation well below the ion scales partly supports the picture that turbulent ion heating mostly occurs at $k_\perp \rho_i \sim 1$ and within the first few subion scales [see, e.g., 60,61]. This scenario is further supported by the trends of derivative of the energy conversion terms (see the Supplemental Material [58]).

IV. CONCLUSIONS

Exploiting the space-filter techniques, we have shown that magnetic reconnection and the consequent island dynamics is associated with (i) the onset of a quasisteady turbulent state, and (ii) the emergence of a dual (direct and inverse) transfer of energy originating from subion scales. In the case under study, the observed bidirectional energy flux is characterized by a sign switch of the total flux $\langle \mathcal{S}_{\text{tot}} \rangle$ at around $kd_i \sim 3$, preceded by another change of sign close to $kd_i \sim 1$ connecting subion and MHD dynamics. The MHD regime is indeed characterized by a forward energy transfer, driven by the ion-kinetic-energy channel, as expected for a plasma whose velocity field is forced at large scale. In particular, we found that the dual total energy flux is dominated by the magnetic-energy channel, which is driven by the interaction between the large-scale electron-current density and the "turbulent" Hall electric field $\widehat{\boldsymbol{j}}_e \cdot \boldsymbol{\epsilon}_{\text{Hall}}^*$. The existence of a simultaneous direct and inverse transfer at subion scales, driven by magnetic reconnection, may have fundamental implications on our understanding of turbulent ion heating in the solar wind [62,63], especially in the context of the so-called "helicity barrier" [21,22,64,65] and in the interpretation of solar wind intermittent dynamics in terms of the interplay of structures and waves [19]. Moreover, while in our setup the sub-ion-scale dual transfer involves "ion-coupled" magnetic reconnection (i.e., reconnection events that develop ion outflows), we believe that an analogous picture would hold also when turbulence is dominated by "electron-only" reconnection events [59,66,67]; we indeed mention that a preprint addressing a similar issue in the context of electron-only reconnection in merging (sub-ion-scale) flux tubes appeared in [68] while we were in the resubmission stage of the present manuscript, further supporting the robustness of our results. In general, we conjecture that a sub-ion-scale dual energy transfer would develop regardless of the microphysics at play in the reconnecting layer, i.e., independently of the details underlying magnetic reconnection at kinetic scales, provided
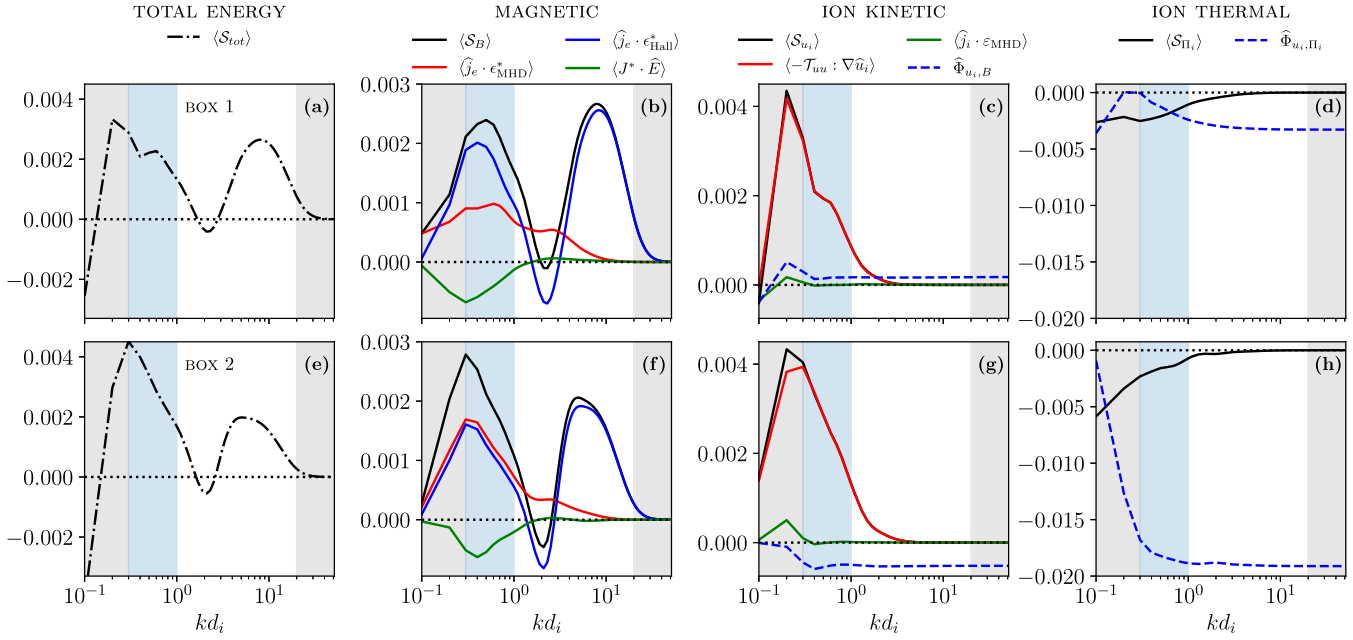
FIG. 3. Energy transfer terms computed within box 1 and 2 indicated Fig. 1 and averaged from $t \approx 165\Omega_{c,i}^{-1}$ to $t \approx 200\Omega_{c,i}^{-1}$. Panels (a)–(d) refer to box 1 and show total, magnetic, ion-kinetic, and ion-thermal energy transfer components. The same quantities are displayed in panels (e)–(h) for box 2. Gray-shaded regions denotes the wavenumber ranges affected by the external forcing ($kd_i \lesssim 0.3$) and by numerical dissipation ($kd_i \gtrsim 20$). Blue-shaded areas indicate the MHD range.

that the separation between ion scales and the collisionless reconnection scale is large enough.

[1] O. Alexandrova, J. Saur, C. Lacombe, A. Mangeney, J. Mitchell, S. J. Schwartz, and P. Robert, Phys. Rev. Lett. **103**, 165003 (2009).

[2] F. Sahraoui, M. L. Goldstein, P. Robert, and Y. V. Khotyaintsev, Phys. Rev. Lett. **102**, 231102 (2009).

[3] C. H. K. Chen, T. S. Horbury, A. A. Schekochihin, R. T. Wicks, O. Alexandrova, and J. Mitchell, Phys. Rev. Lett. **104**, 255002 (2010).

[4] R. Bruno and D. Telloni, Astrophys. J. Lett. **811**, L17 (2015).

[5] C. H. K. Chen and S. Boldyrev, Astrophys. J. **842**, 122 (2017).

[6] T. Wang, J. He, O. Alexandrova, M. Dunlop, and D. Perrone, Astrophys. J. **898**, 91 (2020).

[7] R. Marino and L. Sorriso-Valvo, Phys. Rep. **1006**, 1 (2023).

[8] L. Franci, S. Landi, L. Matteini, A. Verdini, and P. Hellinger, Astrophys. J. **812**, 21 (2015).

[9] T. N. Parashar, W. H. Matthaeus, M. A. Shay, and M. Wan, Astrophys. J. **811**, 112 (2015).

[10] S. S. Cerri, F. Califano, F. Jenko, D. Told, and F. Rincon, Astrophys. J. Lett. **822**, L12 (2016).

[11] L. Franci, S. Landi, L. Matteini, A. Verdini, and P. Hellinger, Astrophys. J. **833**, 91 (2016).

[12] S. S. Cerri, S. Servidio, and F. Califano, Astrophys. J. Lett. **846**, L18 (2017).

[13] D. Grošelj, S. S. Cerri, A. Bañón Navarro, C. Willmott, D. Told, N. F. Loureiro, F. Califano, and F. Jenko, Astrophys. J. **847**, 28 (2017).

[14] S. S. Cerri, M. W. Kunz, and F. Califano, Astrophys. J. Lett. **856**, L13 (2018).

[15] D. Grošelj, A. Mallet, N. F. Loureiro, and F. Jenko, Phys. Rev. Lett. **120**, 105101 (2018).

[16] D. Perrone, T. Passot, D. Laveder, F. Valentini, P. L. Sulem, I. Zouganelis, P. Veltri, and S. Servidio, Phys. Plasmas **25**, 052302 (2018).

[17] L. Arzamasskiy, M. W. Kunz, B. D. G. Chandran, and E. Quataert, Astrophys. J. **879**, 53 (2019).

[18] S. S. Cerri, D. Grošelj, and L. Franci, Front. Astron. Space Sci. **6**, 64 (2019).

[19] D. Grošelj, C. H. K. Chen, A. Mallet, R. Samtaney, K. Schneider, and F. Jenko, Phys. Rev. X **9**, 031037 (2019).

[20] S. S. Cerri, L. Arzamasskiy, and M. W. Kunz, Astrophys. J. **916**, 120 (2021).

[21] T. Passot, P. L. Sulem, and D. Laveder, J. Plasma Phys. **88**, 905880312 (2022).

[22] J. Squire, R. Meyrand, M. W. Kunz, L. Arzamasskiy, A. A. Schekochihin, and E. Quataert, Nat. Astron. **6**, 715 (2022).

[23] S. S. Cerri and F. Califano, New J. Phys. **19**, 025007 (2017).

[24] L. Franci, S. S. Cerri, F. Califano, S. Landi, E. Papini, A. Verdini, L. Matteini, F. Jenko, and P. Hellinger, Astrophys. J. Lett. **850**, L16 (2017).

[25] D. Vech, A. Mallet, K. G. Klein, and J. C. Kasper, Astrophys. J. Lett. **855**, L27 (2018).

[26] C. Dong, L. Wang, Y.-M. Huang, L. Comisso, and A. Bhattacharjee, Phys. Rev. Lett. **121**, 165101 (2018).

[27] E. Papini, L. Franci, S. Landi, A. Verdini, L. Matteini, and P. Hellinger, Astrophys. J. **870**, 52 (2019).

[28] A. Tenerani and M. Velli, MNRAS **491**, 4267 (2020).

[29] D. Borgogno, D. Grasso, B. Achilli, M. Romé, and L. Comisso, Astrophys. J. **929**, 62 (2022).

[30] C. Dong, L. Wang, Y.-M. Huang, L. Comisso, T. A. Sandstrom, and A. Bhattacharjee, Sci. Adv. **8**, eabn7627 (2022).

[31] S. S. Cerri, T. Passot, D. Laveder, P. L. Sulem, and M. W. Kunz, Astrophys. J. **939**, 36 (2022).

[32] M. Germano, J. Fluid Mech. **238**, 325 (1992).

[33] C. Meneveau and J. Katz, Annu. Rev. Fluid Mech. **32**, 1 (2000).

[34] H. Aluie and G. L. Eyink, Phys. Rev. Lett. **104**, 081101 (2010).

[35] P. Morel, A. B. Navarro, M. Albrecht-Marc, D. Carati, F. Merz, T. Görler, and F. Jenko, Phys. Plasmas **18**, 072301 (2011).

[36] M. Miesch, W. Matthaeus, A. Brandenburg, A. Petrosyan, A. Pouquet, C. Cambon, F. Jenko, D. Uzdensky, J. Stone, S. Tobias, J. Toomre, and M. Velli, Space Sci. Rev. **194**, 97 (2015).

[37] Y. Yang, W. H. Matthaeus, T. N. Parashar, P. Wu, M. Wan, Y. Shi, S. Chen, V. Roytershteyn, and W. Daughton, Phys. Rev. E **95**, 061201 (2017).

[38] Y. Yang, W. H. Matthaeus, T. N. Parashar, C. C. Haggerty, V. Roytershteyn, W. Daughton, M. Wan, Y. Shi, and S. Chen, Phys. Plasmas **24**, 072306 (2017).

[39] E. Camporeale, L. Sorriso-Valvo, F. Califano, and A. Retinò, Phys. Rev. Lett. **120**, 125101 (2018).

[40] S. S. Cerri and E. Camporeale, Phys. Plasmas **27**, 082102 (2020).

[41] S. Adhikari, T. N. Parashar, M. A. Shay, W. H. Matthaeus, P. S. Pyakurel, S. Fordin, J. E. Stawarz, and J. P. Eastwood, Phys. Rev. E **104**, 065206 (2021).

[42] A. Alexakis and S. Chibbaro, J. Plasma Phys. **88**, 905880515 (2022).

[43] G. Arró, F. Califano, and G. Lapenta, Astron. &Astrophys. **668**, A33 (2022).

[44] D. Manzini, F. Sahraoui, and F. Califano, Phys. Rev. Lett. **130**, 205201 (2023).

[45] A. Alexakis and L. Biferale, Phys. Rep. **767-769**, 1 (2018).

[46] R. Marino, P. D. Mininni, D. Rosenberg, and A. Pouquet, EPL (Europhysics Letters) **102**, 44006 (2013).

[47] R. Marino, A. Pouquet, and D. Rosenberg, Phys. Rev. Lett. **114**, 114504 (2015).

[48] D. Balwada, J.-H. Xie, R. Marino, and F. Feraco, Sci. Adv. **8**, eabq2566 (2022).

[49] A. Alexakis, R. Marino, P. D. Mininni, A. van Kan, R. Foldes, and F. Feraco, Science **383**, 1005 (2024).

[50] R. Foldes, E. Lêvêque, R. Marino, E. Pietropaolo, A. De Rosis, D. Telloni, and F. Feraco, J. Plasma Phys. **89**, 905890413 (2023).

[51] V. Carbone, L. Sorriso-Valvo, and R. Marino, Europhys. Lett. **88**, 25001 (2009).

[52] R. Marino, L. Sorriso-Valvo, R. D'Amicis, V. Carbone, R. Bruno, and P. Veltri, Astrophys. J. **750**, 41 (2012).

[53] L. Sorriso-Valvo, R. Marino, L. Lijoi, S. Perri, and V. Carbone, Astrophys. J. **807**, 86 (2015).

[54] L. Franci, S. Landi, A. Verdini, L. Matteini, and P. Hellinger, Astrophys. J. **853**, 26 (2018).

[55] S. S. Cerri, L. Franci, F. Califano, S. Landi, and P. Hellinger, J. Plasma Phys. **83**, 705830202 (2017).

[56] The Movie at http://link.aps.org/supplemental/10.1103/PhysRevE.110.055207 displays the temporal evolution of the quantities presented in Fig. 1 (2024).

[57] S. Lu, Q. Lu, R. Wang, X. Li, X. Gao, K. Huang, S. Haomin, Y. Yang, A. Artemyev, X. An, and Y. Jia, Astrophys. J. **943**, 100 (2023).

[58] See Supplemental Material at http://link.aps.org/supplemental/10.1103/PhysRevE.110.055207 for details on the spatial correlation between the inverse energy flux and the current density structures; the full-volume-averaged filtered quantities; the filtered terms of the energy channels computed in the three sub-domains of Fig. 1; the filtered terms concerning ion-kinetic and ion-thermal energy exchanges and ion-kinetic and magnetic energy exchanges, which includes Refs. [69–77].

[59] F. Califano, S. S. Cerri, M. Faganello, D. Laveder, M. Sisti, and M. W. Kunz, Front. Phys. **8**, 317 (2020).

[60] A. A. Schekochihin, S. C. Cowley, W. Dorland, G. W. Hammett, G. G. Howes, E. Quataert, and T. Tatsuno, Astrophys. J. Suppl. Series **182**, 310 (2009).

[61] B. D. G. Chandran, B. Li, B. N. Rogers, E. Quataert, and K. Germaschewski, Astrophys. J. **720**, 503 (2010).

[62] R. Marino, L. Sorriso-Valvo, V. Carbone, A. Noullez, R. Bruno, and B. Bavassano, Astrophys. J. Lett. **677**, L71 (2008).

[63] R. Marino, L. Sorriso-Valvo, V. Carbone, P. Veltri, A. Noullez, and R. Bruno, Planet. Space Sci. **59**, 592 (2011).

[64] T. Passot and P. L. Sulem, J. Plasma Phys. **85**, 905850301 (2019).

[65] R. Meyrand, J. Squire, A. A. Schekochihin, and W. Dorland, J. Plasma Phys. **87**, 535870301 (2021).

[66] P. Sharma Pyakurel, M. A. Shay, T. D. Phan, W. H. Matthaeus, J. F. Drake, J. M. TenBarge, C. C. Haggerty, K. G. Klein, P. A. Cassak, T. N. Parashar, M. Swisdak, and A. Chasapis, Phys. Plasmas **26**, 082307 (2019).

[67] C. Granier, S. S. Cerri, and F. Jenko, Astrophys. J. **974**, 11 (2024).

[68] Z. Liu, C. Silva, L. M. Milanese, M. Zhou, N. R. Mandell, and N. F. Loureiro, arXiv:2407.06020.

[69] J. F. Drake, M. Swisdak, T. D. Phan, P. A. Cassak, M. A. Shay, S. T. Lepri, R. P. Lin, E. Quataert, and T. H. Zurbuchen, J. Geophys. Res. **114**, A05111 (2009).

[70] J. Yoo, M. Yamada, H. Ji, and C. E. Myers, Phys. Rev. Lett. **110**, 215007 (2013).

[71] A. Bañón Navarro, B. Teaca, D. Told, D. Groselj, P. Crandall, and F. Jenko, Phys. Rev. Lett. **117**, 245101 (2016).

[72] S. Usami, R. Horiuchi, and H. Ohtani, Phys. Plasmas **24**, 092101 (2017).

[73] Y. D. Yoon and P. M. Bellan, Astrophys. J. Lett. **868**, L31 (2018).

[74] M. A. Shay, C. C. Haggerty, W. H. Matthaeus, T. N. Parashar, M. Wan, and P. Wu, Phys. Plasmas **25**, 012304 (2018).

[75] D. Villa, N. Dubuit, O. Agullo, A. Poyé, X. Garbet, and A. Smolyakov, J. Plasma Phys. **88**, 905880613 (2022).

[76] Z. Wu, J. He, D. Duan, X. Zhu, C. Hou, D. Verscharen, G. Nicolaou, C. J. Owen, A. Fedorov, and P. Louarn, Astrophys. J. **951**, 98 (2023).

[77] M. Sadek and H. Aluie, Phys. Rev. Fluids **3**, 124610 (2018).